Astronomy & Astrophysics

The diameters of α Centauri A and B

A comparison of the asteroseismic and VINCI/VLTI views

P. Kervella[1], F. Thévenin[2], D. Ségransan[3], G. Berthomieu[2], B. Lopez[4], P. Morel[2], and J. Provost[2]

[1] European Southern Observatory, Alonso de Cordova 3107, Casilla 19001, Santiago 19, Chile
[2] Département Cassini, UMR CNRS 6529, Observatoire de la Côte d'Azur, BP 4229, 06304 Nice Cedex 4, France
[3] Observatoire de Genève, 1290 Sauverny, Switzerland
[4] Département Fresnel, UMR CNRS 6528, Observatoire de la Côte d'Azur, BP 4229, 06304 Nice Cedex 4, France

Abstract. We compare the first direct angular diameter measurements obtained on our closest stellar neighbour, α Centauri, to recent model diameters constrained by asteroseismic observations. Using the VINCI instrument installed at ESO's VLT Interferometer (VLTI), the angular diameters of the two main components of the system, α Cen A and B, were measured with a relative precision of 0.2% and 0.6% respectively. Particular care has been taken in the calibration of these measurements, considering that VINCI is estimating the fringe visibility using a broadband K filter. We obtain uniform disk angular diameters for α Cen A and B of $\theta_{\rm UD}[{\rm A}] = 8.314 \pm 0.016$ mas and $\theta_{\rm UD}[{\rm B}] = 5.856 \pm 0.027$ mas, and limb darkened angular diameters of $\theta_{\rm LD}[{\rm A}] = 8.511 \pm 0.020$ mas and $\theta_{\rm LD}[{\rm B}] = 6.001 \pm 0.034$ mas. Combining these values with the parallax from Söderhjelm (1999), we derive linear diameters of $D[{\rm A}] = 1.224 \pm 0.003\ D_\odot$ and $D[{\rm B}] = 0.863 \pm 0.005\ D_\odot$. These values are compatible with the masses published by Thévenin et al. (2002) for both stars.

Key words. techniques: interferometric – stars: binaries: visual – stars: evolution – stars: oscillations – stars: fundamental parameters – stars: individual: α Cen

1. Introduction

The α Centauri triple star system is our closest stellar neighbour. The main components are G2V and K1V solar-like stars, while the third member is the red dwarf *Proxima* (M5.5V). α Cen A (HD 128620) and B (HD 128621) offer the unique possibility to study the stellar physics at play in conditions just slightly different from the solar ones. Their masses bracket nicely the Sun's value, while they are slightly older. In spite of their high interest, proximity and brightness, the two main components have never been resolved by long baseline stellar interferometry, due to their particularly southern position in the sky. We report in this paper the first direct measurement of their angular diameters. As a remark, the angular diameter of *Proxima* has also been measured recently for the first time ($\theta_{\rm LD} = 1.02 \pm 0.08$ mas) using two 8-meters Unit Telescopes and the VINCI instrument (Ségransan et al. 2003).

More than fourty years after the discovery of the solar seismic frequencies by Leighton (1960), and Evans & Michard (1962), solar-like *p* oscillations have been identified on α Cen A & B by Bouchy & Carrier (2001, 2002) with the CORALIE fiber-fed spectrograph. Today, asteroseismic frequencies have been detected in several additional stars. All these observations provide constraints, on one hand on stellar interior studies, and on the other hand on macroscopic stellar parameters like mass and radius. Several binary systems like α Cen (see Morel et al. 2001 for references) have been calibrated using spectro-photometry constraints. Recently, α Cen A has been calibrated using photometry, astrometry, spectroscopy and asteroseismic frequencies (Thévenin et al. 2002). These authors derived the age of the couple, the initial helium abundance Y_i, and the radii of both stars. This calibration was based on stellar evolution models computed using the CESAM code (Morel 1997). One of the main results of this calibration was to constrain the masses of both stars, and in particular the mass of B. It had to be diminished by 3%, compared to the mass proposed by Pourbaix et al. (2002), leading to a smaller diameter of the star B. The high precision interferometric measurements of the angular diameters of α Cen A and B with VINCI/VLTI are a direct test of these refined models.

2. Depscription of the instrument

2.1. The VLT Interferometer and VINCI

The European Southern Observatory's Very Large Telescope Interferometer (Glindemann et al. 2000) is operated on top of the Cerro Paranal, in Northern Chile, since March 2001.

In its current state of completion, the light coming from two telescopes can be combined coherently in VINCI, the VLT Interferometer Commissioning Instrument (Kervella et al. 2000, 2003a), or in the mid-infrared instrument MIDI (Leinert et al. 2000). A three ways beam combiner, AMBER (Petrov et al. 2000), will soon be installed in addition to these instruments. VINCI uses in general a regular K band filter ($\lambda = 2.0-2.4\ \mu$m), as this was the case for our α Cen observations, but can also be operated in the H band ($\lambda = 1.4-1.8\ \mu$m) using an integrated optics beam combiner (Berger et al. 2001). The K band setup effective wavelength changes slightly, depending on the spectral type of the observed target, between 2.174 and 2.184 μm for $3000 \leq T_{\text{eff}} \leq 100\,000$ K. For α Cen A and B, $\lambda_{\text{eff}} = 2.178 \pm 0.003\ \mu$m (see Sect. 3.3 for details).

2.2. Interferometer configuration

We used as primary light collectors the two 0.35 m Test Siderostats of the VLTI. After being delayed by the VLTI optical delay lines, the stellar light was recombined in the interferometric laboratory using the VINCI instrument. A large number of baselines are accessible on the Cerro Paranal summit. Two of them were used for this study: E0-G0 and E0-G1, respectively of 16 and 66 meters ground length. The 16 m baseline observations were obtained during the early commissioning phase, from two days to a few weeks after the first fringes in March 2001. At the time, the effective aperture of the siderostats was limited to 0.10 m due to the unavailability of optical beam compression devices. Later in 2001, their installation allowed to recover the full 0.35 m primary mirror aperture of the siderostats, and all the 66 m baseline observations reported here were done with the full mirror. The shorter 16 m baseline is useful in the case of α Cen A to determine unequivocally the position of the 66 m measurements on the visibility curve, but does not bring a significant contribution to the final angular diameter precision (see Sect. 7).

2.3. Visibility calibration

During observations, the interferometric efficiency (visibility produced by the system when observing a point source) varies slowly over a timescale of hours. This means that the scientific target observations have to be calibrated periodically using observations of a star with a known angular diameter. The data reduction software of VINCI yields accurate estimates of the squared modulus of the coherence factor μ^2, which is linked to the object visibility V by the relationship

$$V^2 = \frac{\mu^2}{T^2} \tag{1}$$

where T is the interferometric efficiency. T is estimated by bracketing the science target with observations of calibrator stars whose V is supposed to be known a priori. The precision of our knowledge of the calibrator's angular diameter is therefore decisive for the final quality of the calibrated visibility value. For our observations, we have applied a constant transfer function T^2 between calibrator stars. This assumption

has been validated during routine VLTI observations. A detailed description of the calibration observations can be found in Sect. 4.

3. Data processing

3.1. Data processing algorithm

We used a customized version of the standard VINCI data reduction pipeline (Kervella et al. 2003b), whose general principle is based on the original FLUOR algorithm (Coudé du Foresto et al. 1997). The two calibrated output interferograms are subtracted to remove residual photometric fluctuations. We implemented in this code a time-frequency analysis (Ségransan et al. 1999) based on the continuous wavelet transform (Farge 1992). Instead of the projection of the signal onto a sine wave of the Fourier transform, the wavelet transform decomposes it onto a function, i.e. the wavelet, that is localised in both time and frequency. We used as a basis the Morlet wavelet, a Gaussian envelope multiplied by a sinus wave. With the proper choice of the number of oscillations inside the Gaussian envelope, the Morlet wavelet closely matches a VINCI interferogram. It is therefore very efficient at localizing the signal in both time and frequency.

3.2. Data quality control

In spite of the relatively high modulation frequency of the fringes (296 Hz for the 66m baseline measurements), a fraction of the recorded interferograms present a differential piston signature between the two apertures. This is due to the relatively low coherence time observed at Paranal (1–4 ms at $\lambda = 500$ nm). These interferograms are rejected in the VINCI data processing by comparing the frequency of the measured fringe peak with the expected frequency from the K band filter of VINCI. If the measured fringe frequency is different by more than 20% from the expected frequency, the interferogram is ignored. The fringe packet extensions in the time and frequency domains are also used for the selection. This process allows to keep only the best quality interferograms and reduces the final dispersion of the visibilities. Finally, we rejected the observations that presented an abnormally low photometric signal to noise ratio, that is a typical symptom of an inaccuracy in the pointing of the siderostats.

The total numbers of selected and processed interferograms are 7854 on α Cen A (2427 on the 66 m baseline and 5427 on the 16 m baseline) and 1833 on α Cen B (66 m baseline only). For the calibration of the α Cen observations, we processed 2998 interferograms of θ Cen. Several calibrators (including θ Cen) were used for the 16 m baseline measurements of α Cen A, for a total of 8059 processed interferograms. The separate measurement of θ Cen was achieved using 1750 interferograms of this star and 789 interferograms of the secondary calibrator 58 Hya.

After the processing of a series of interferograms (100 to 500 scans), the mean squared coherence factor is derived from the average wavelets power spectral density of the selected interferograms. Figure 1 shows the average wavelets
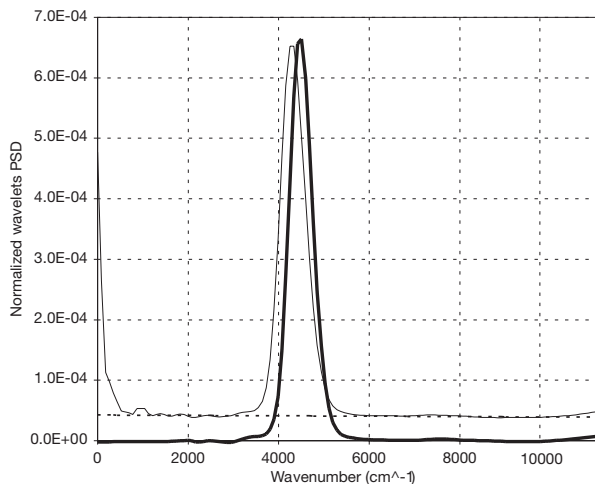
Fig. 1. Wavelets power spectral density (PSD) of a processed series of 418 interferograms obtained on α Cen A, before (thin line) and after (thick line) recentering of the fringe peak and subtraction of the background noise (dashed line).

power spectral density (PSD) of 418 processed interferograms, summed over the time extent of the fringe packet to obtain a one dimensional vector. In spite of the very low visibility of the fringes of α Cen A on the 66 m baseline ($V^2 \simeq 1\%$), the fringe peak is well defined.

The noise background (residual detector and photon shot noise) is estimated directly from the higher and lower frequencies of the average PSD of the interferogram, and then subtracted. As shown in Fig. 1, the subtraction is very efficient and gives a clean final PSD. The individual interferogram PSDs are summed after recentering of the fringe peak maximum, to reduce the power spread due to piston effect. This avoids that energy is lost in the integration process and allows a more precise estimation of the background level. We have chosen not to use the background removal method described by Perrin (2003), as we are simultaneously removing both the photon shot noise and detector noise contributions.

In Fig. 1, the recentered and background corrected fringe peak is shifted slightly towards higher wavenumber values due to the variation of α Cen A visibility over the K band. For simplicity reasons, the data reduction software assumes a fixed wavelength of 2.195 μm of the fringe peak maximum for the recentering process for all stars, but the exact target value has no effect on the final visibility.

3.3. Instrumental transmission

3.3.1. Transmission model

When using VINCI, the observations are carried out using a full K band filter, accepting the star light from 2.0 to 2.4 μm. In order to obtain a precise fit of the calibrated visibilities measured on sky, we computed the transmission of the interferometer taking into account the atmospheric transmission (Lord 1992), the fluoride glass optical fibers, the K band filter and the quantum efficiency of the HAWAII detector. This gave us a first approximation of the transmission of the interferometer $F_0(\lambda)$.

Table 1. Determination of the transmission correction slope γ of the VINCI/VLTI combination as observed on bright stars with two 8-meters telescopes.

|	Peak position (μm)	γ (μm^{-1})
α PsA	2.198 ± 0.002	1.140
HR 8685 (1)	2.190 ± 0.003	0.911
HR 8685 (2)	2.202 ± 0.008	1.119
γ^2 Vol	2.198 ± 0.007	1.076
ϵ Eri	2.197 ± 0.010	1.065
39 Eri	2.196 ± 0.010	1.076
	Weighted average	1.076 ± 0.081

3.3.2. On-sky calibration

The instrumental uncertainties led us to compare directly this theoretical VINCI/VLTI transmission model to the real transmission of the system on sky. This has been achieved through the precise estimation of the effective wavenumber of a series of bright stars observations obtained with VINCI and two 8 meters Unit Telescopes (Table 1). A multiplicative slope γ (expressed in μm^{-1}) is superimposed to the theoretical transmission $F_0(\lambda)$ in order to match the observed average position of the PSD fringe peak. It is the only variable adjusted to match the observations. The photometric signal to noise ratio of the UTs observations being very high, we obtain a good precision on the average fringe peak frequency and thus on the estimation of γ, as shown in Table 1. The total photometric transmission of the interferometer $F(\lambda)$ is then given by:

$$F(\lambda) = \gamma(\lambda - \lambda_0) \, F_0(\lambda). \tag{2}$$

The reference wavelength λ_0 was set arbitrarily to 1.90 μm in our computation, but has no influence on the transmission calibration. $F(\lambda)$ is not normalized and gives only relative transmission values over the K band, but the absolute transmission is not needed to derive the model visibilities. It should be stressed that the sensitivity of the final angular diameter to γ is low, a ±0.08 μm^{-1} change of this parameter resulting only in a ±0.010 mas change on θ_{UD} for α Cen A, and ±0.007 mas for B. These uncertainties were quadratically added to the final errors of the UD and LD angular diameter values given further in this paper. As a remark, we can also express this as a ±0.003 μm uncertainty on the average value of $\lambda_{eff} = 2.178$ μm that we derive from $F(\lambda)$ for α Cen A and B.

3.3.3. Discussion

The observations of α Cen have been obtained with the siderostats, that have a slightly different optical setup than the UTs. There are 26 reflections for the UTs configuration in each arm of the interferometer, compared to 20 for the siderostats. Out of these, 15 mirrors are common between the two configurations. The remaining difference is therefore between the additional 11 reflections of the UTs and the additional 5 reflexions of the siderostats. Even assuming a very conservative mismatch of 1% between the extreme wavelengths reflectivity of each mirror of the UT train compared to the siderostats, we obtain a relative difference on γ of only 3%
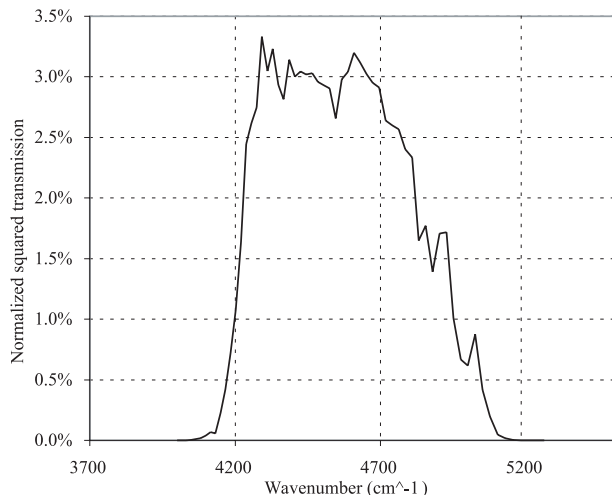
Fig. 2. Model PSD of α Cen A fringes for a zero baseline, including the spectrum of the star, atmosphere, fluoride glass fibers, K band filter, detector quantum efficiency and the correction function $F_1(\lambda)$ (see Sect. 3.3). A total precipitable water vapor of 3.0 mm (median for Paranal) is assumed for this plot. The curve for α Cen B is almost identical.

that is significantly less than our quoted statistical uncertainty (7.5%). We have therefore considered this diffference negligible in our study.

A possible reason for the observed wavelength drift is the aging of the 20 mirror coatings necessary to bring the star light into the VINCI instrument (for each of the two beams). This process may have affected differentially the reflectivity of one end of the K band compared to the other. A difference in reflectivity of only 1% between the two extreme wavelengths will result in an 18% difference on the final transmission, after 20 mirrors (siderostats configuration). Also, the transmission curves provided by the manufacturer of the fiber optics used in VINCI do not have a sufficient precision to constrain accurately the instrument transmission model, and an error of several tens of percent is not to be excluded. To a lesser extent, the engineering grade HAWAII infrared array used in VINCI may have a quantum efficiency curve differing from the science grade versions by several percent. Finally, the MONA triple coupler used to recombine the light has also shown some birefringence during laboratory tests. This effect could result in a shift of the effective observation wavelength.

To secure the internal wavelength calibration of VINCI itself, crucial for the accuracy of the estimation of γ, we have obtained laboratory fringes with a K band laser ($\lambda = 2.304$ μm). This gave us a precise wavelength reference to verify the scanning speed and the camera acquisition frequency.

3.3.4. Source spectrum

In addition to the constant term of the instrumental transmission, the shape of the source spectrum for each star was taken into account using its effective temperature. We computed synthetic spectra for α Cen A and B using Kurucz models, but considering the absence of any large absorption feature in the K band, we did not include spectral features in our
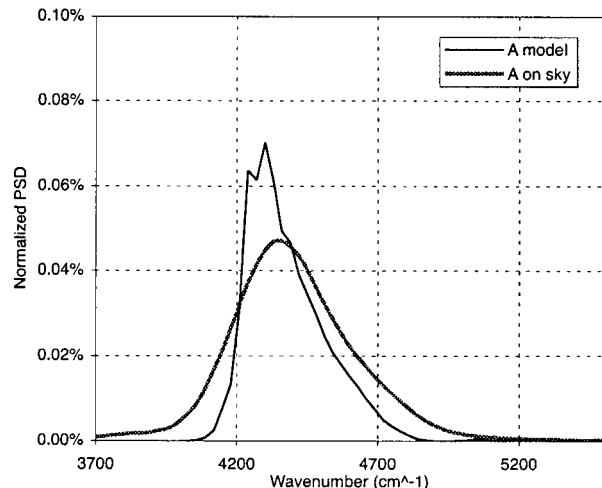
Fig. 3. Model (black line) and observed (grey line) PSDs of α Cen A fringes on the 66m baseline (61 m projected). The visibility loss for larger wavenumbers is clearly visible. The observed Fourier PSD, smoothed by the differential piston, shows the expected asymmetry. The on-sky and model vertical scales are arbitrary.
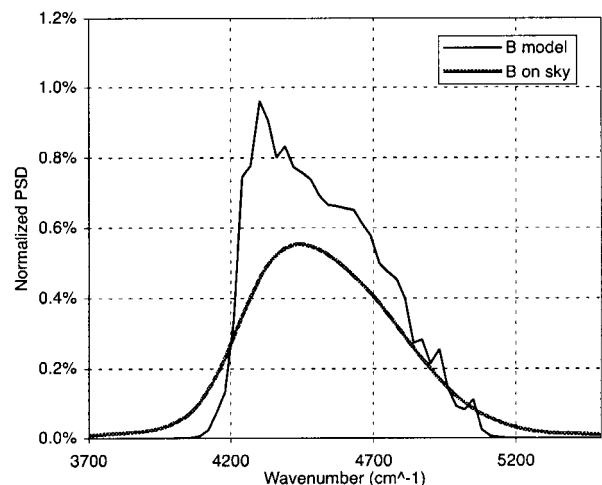
Fig. 4. Model (black line) and observed (grey line) PSDs of α Cen B fringes on the E0-G1 baseline. α Cen B being significantly less resolved than A, the squared visibility is more uniform over the K band than for α Cen A (Fig. 3). The asymmetry of the power spectrum is therefore smaller, though still present. The on-sky and model vertical scales are arbitrary.

final transmission model. The simulated spectrum of α Cen A fringes for a zero baseline is shown in Fig. 2.

3.4. Bandwidth smearing

An important effect of the relatively large spectral bandwidth of the VINCI filter is that several spatial frequencies are observed simultaneously by the interferometer. This effect is called *bandwidth smearing*. In the case of α Cen A, it is particularly strong as the visibilities are close to the first minimum of the visibility function, and this effect cannot be neglected. With a 60 m projected baseline, the short wavelength edge of the K band ($\lambda \simeq 2.0$ μm) is already at the null of visibility, while the V^2 for the long wavelength edge ($\lambda \simeq 2.4$ μm) is still

Table 2. Calibration observations of θ Cen and 58 Hya. The expected visibilities given in this table include the bandwidth smearing effect. The resulting interferometric efficiencies assumed for the calibration of the α Cen and θ Cen observations are given in bold characters, with the corresponding statistical and systematic error bars for each observing session. The calibrated visibilities can be found in Table 3 for θ Cen, and in Tables 5 and 6 for α Cen A and α Cen B.

JD − 2 450 000	Scans	B (m)	Azim. ($N = 0$)	μ^2 (%) ± stat. err.	Expected V^2 (%) ± syst. err.	IE (μ^2/V^2, %) ± stat. ± syst.	Target(s)
						52.08 ± 0.69 ± 0.63	θ Cen
2452.63024	45	65.2509	161.90	30.72 ± 0.75	58.90 ± 0.71	52.17 ± 1.27 ± 0.63	58 Hya
2452.63324	166	65.2011	162.55	31.56 ± 0.74	58.95 ± 0.71	53.54 ± 1.25 ± 0.64	58 Hya
2452.64109	269	65.0719	164.26	30.66 ± 0.31	59.08 ± 0.71	51.91 ± 0.52 ± 0.62	58 Hya
2452.64527	256	65.0047	165.18	30.73 ± 0.37	59.15 ± 0.71	51.95 ± 0.62 ± 0.62	58 Hya
						52.13 ± 0.69 ± 0.63	θ Cen
2452.67563	53	64.5970	174.54	31.42 ± 0.77	59.56 ± 0.70	52.77 ± 1.29 ± 0.62	58 Hya
2462.53152	389	65.7824	153.61	8.58 ± 0.17	18.13 ± 0.28	47.33 ± 0.93 ± 0.72	θ Cen
2462.60245	88	65.8892	168.69	8.63 ± 0.15	18.01 ± 0.27	47.94 ± 0.86 ± 0.73	θ Cen
						47.51 ± 0.49 ± 0.72	α Cen A, α Cen B
2462.60554	283	65.8801	169.39	8.46 ± 0.21	18.02 ± 0.27	46.97 ± 1.18 ± 0.72	θ Cen
2465.56068	94	65.9551	161.27	8.67 ± 0.14	17.93 ± 0.27	48.33 ± 0.80 ± 0.74	θ Cen
2465.56377	355	65.9541	161.93	8.58 ± 0.24	17.93 ± 0.27	47.87 ± 1.31 ± 0.73	θ Cen
2465.57390	241	65.9413	164.14	8.98 ± 0.50	17.95 ± 0.27	50.06 ± 2.80 ± 0.77	θ Cen
2465.57838	317	65.9320	165.13	8.85 ± 0.29	17.96 ± 0.27	49.31 ± 1.64 ± 0.75	θ Cen
						48.64 ± 1.50 ± 0.76	α Cen A, α Cen B
2465.65159	69	65.8006	1.99	9.35 ± 0.44	18.11 ± 0.28	51.66 ± 2.43 ± 0.79	θ Cen
2470.56229	87	65.9373	164.59	9.01 ± 0.13	17.95 ± 0.27	50.19 ± 0.73 ± 0.77	θ Cen
2470.56609	386	65.9289	165.43	9.00 ± 0.05	17.96 ± 0.27	50.09 ± 0.30 ± 0.77	θ Cen
2470.57010	341	65.9188	166.32	9.06 ± 0.15	17.97 ± 0.27	50.44 ± 0.83 ± 0.77	θ Cen
2470.57433	348	65.9073	167.27	8.73 ± 0.14	17.99 ± 0.27	48.53 ± 0.77 ± 0.74	θ Cen
						49.97 ± 0.87 ± 0.76	α Cen A, α Cen B

above 1%. The photons at the null of visibility have interfered destructively. Therefore, the fringe peak becomes very asymmetric in the PSD of the interferograms. As shown in Figs. 3 and 4, the observed and model PSDs agree well in general shape. The on-sky power spectrum is blurred by the differential piston and therefore appears "smoothed", but the characteristic asymmetry for low visibilities is clearly visible.

3.5. Baseline smearing

When the aperture of the light collectors is a significant fraction of the baseline, an effect similar to the bandwidth smearing appears on the visibility measurements. It comes from the fact that the baselines defined between different parts of the two primary mirrors cover a non-zero range of lengths and orientations. Therefore, several spatial frequencies are measured simultaneously by the beam combiner. In the case of the E0-G0 baseline (16 m) observations of α Cen A, the effective aperture was 0.10 m, and therefore the ratio of the primary mirror diameter to the baseline was only $D/B \approx 0.6\%$. For the E0-G1 baseline (66 m), this ratio is similar due to the larger 0.35 m apertures. Even in the difficult case of the α Cen A observations, this effect accounts at most for a relative shift of the visibility of 0.1%, to be compared to our relative systematic calibration error of 1.5%. In the case of α Cen B, we expect at most a 0.05% shift, for a relative systematic calibration error also of 1.5%. We have therefore neglected this effect in the rest of our study.

4. Calibration observations

The calibration of the interferometric efficiency (IE) of the interferometer is a critical step of the observations. We present in Table 2 the measurements that we obtained on the calibrators and the corresponding values of the IE for the three nights of observations of the α Cen pair (JD = 2 452 462-70) on the E0-G1 baseline, and the separate night used to measure θ Cen (JD = 2452452).

The primary calibrator θ Cen is located at a distance of 24 degrees from the α Cen pair, mostly in declination, while only 9 degrees separate θ Cen and the secondary calibrator 58 Hya. During the observations, the largest difference between the altitudes of θ Cen and α Cen happens at the crossing of the meridian, and is approximately 24 degrees (respective altitudes of about 55 and 80 degrees at Paranal). The airmasses of the two stars at meridian crossing are 1.25 and 1.03 respectively for α Cen and θ Cen. The difference is even smaller in the case of 58 Hya and θ Cen. As we obtained the E0-G1 baseline observations close to the meridian crossing, we do not expect any significant variation of IE due to the difference of airmass between the calibrators and the scientific targets.

5. The primary calibrator θ Centauri

The most important calibrator for the 66 meters baseline measurements is the giant star θ Cen (K0III). This calibrator was chosen for its stability and brightness in the list of standard stars compiled by Cohen et al. (1999) and verified by

Table 3. θ Cen squared visibilities.

JD − 2 450 000	B (m)	Azim. ($N = 0$)	V^2 (%) ± stat. ± syst.
E0-G1			
2452.60644	65.9464	163.49	17.74 ± 0.69 ± 0.21
2452.60943	65.9413	164.15	17.86 ± 0.36 ± 0.22
2452.61396	65.9318	165.15	17.72 ± 0.34 ± 0.21
2452.61906	65.9193	166.28	18.08 ± 0.29 ± 0.22
2452.65518	65.8220	174.54	18.20 ± 0.38 ± 0.22
2452.65855	65.8156	175.32	18.25 ± 0.40 ± 0.22
2452.66275	65.8088	176.30	18.08 ± 0.38 ± 0.22
2452.66685	65.8037	177.26	18.13 ± 0.39 ± 0.22
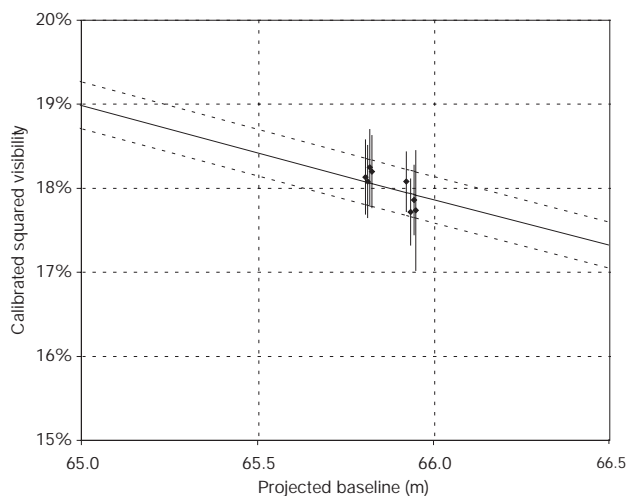
Fig. 5. Detail of θ Cen squared visibilities and uniform disk model. The continuous line is the UD diameter fit (5.305 ± 0.020 mas), and the dotted lines represent the limits of the ±1σ error domain.

Bordé et al. (2002). This choice is critical in the sense that any departure of the true visibility of the calibrator from the assumed model will contaminate the calibrated visibility of the scientific target. This is the reason why one should avoid to use as calibrators pulsating variables (such as many M type giants, Cepheids,...), double or multiple stars, magnetically active objects (photospheric spots) or fast rotators (ellipticity of the star disk). The properties of all the stars listed in the Cohen et al. (1999) catalogue have been checked carefully and their diameters are believed to be constant to a very good accuracy. In addition, θ Cen is not classified as double, variable or active in any catalogue, and is a slow rotator ($V \sin i$ = 1.2 km s^{-1}, Glebocki et al. 2000).

Unfortunately, the typical 1% precision of the Cohen et al. (1999) catalogue on the angular diameters, though very good in itself, is not sufficient due to the large size of this star and the correspondingly low visibility on the 66 meters baseline. After the first processing of our α Cen data, it appeared that the error bars on the final angular diameters were dominated by the systematic uncertainty on the angular size of θ Cen. Therefore, we reduced additional archived data obtained on θ Cen on a separate night, using the secondary calibrator 58 Hya and the 66 meters baseline. 58 Hya has a much smaller angular diameter than θ Cen and therefore provides a precise calibration

Table 4. Parameters of the primary (θ Cen) and secondary (58 Hya) calibrators.

	θ Cen HD 123139	58 Hya HD 130694
m_V	2.06	4.42
m_K	−0.10	1.13
Spectral type	K0IIIb	K4III
T_{eff} (K)[a]	4980	4040
Measurement λ (μm)	2.181	2.181
$\log g$ [a]	2.75	1.85
θ_{LD} (mas)[b]	5.46 ± 0.058	3.22 ± 0.035
θ_{UD} (mas)[c]	5.33 ± 0.057	3.12 ± 0.034
Measured θ_{UD} (mas)	**5.305 ± 0.020**	

[a] T_{eff} and $\log g$ from Cayrel de Strobel et al. (1997).
[b] Catalogue value from Cohen et al. (1999).
[c] Linear limb darkening from Claret (2000).

of the interferometric efficiency. The calibrated squared visibility values obtained on θ Cen are listed in Table 3, and the angular diameter fit is shown in Fig. 5. The parameters for both stars and the measured uniform disk (UD) angular diameter of θ Cen are presented in Table 4. The VINCI/VLTI angular diameter found for this star agrees very well with the Cohen et al. (1999) value, while reducing significantly its uncertainty.

6. Calibrated visibilities

The list of the observations of α Cen A and B, with the resulting calibrated squared visibilities, is presented in Tables 5 and 6. The azimuth of the projected baseline is counted clockwise (cw) from north, and corresponds to the baseline orientation as seen from the star. Two error bars are given for each V^2 value:

– one statistical error bar, computed from the dispersion of the visibility values obtained during the observation,
– one systematic error bar defined by the uncertainty on the knowledge of the calibrator angular size.

While the statistical error can be diminished by repeatedly observing the target, the systematic error cannot be reduced by averaging measurements obtained using the same calibrator. This is taken into account in our model fitting by checking that the final uncertainty of the fit is larger than the systematic errors of each measured visibility value. This conservative approach ensures that we are not underestimating the systematic calibration errors.

## 7. Angular diameters

7.1. Uniform disk

Due to the spectrum shape variation with baseline described in Sect. 3.4, the classical monochromatic uniform disk (UD) model visibility curve is not applicable and can lead to very large UD size errors for low visibilities. We therefore adopted a direct fitting method in the broadband regime. For this
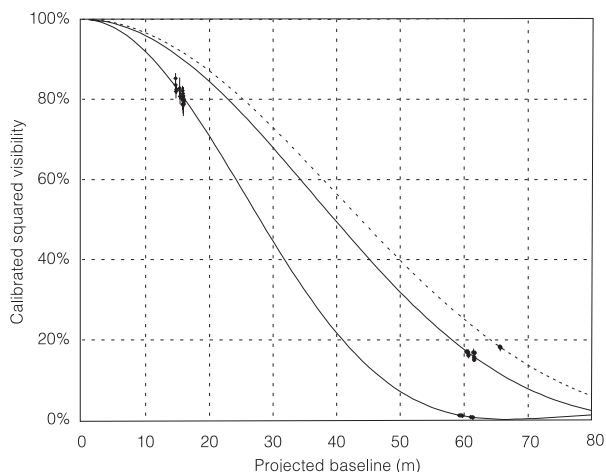
Fig. 6. Overview of the α Cen and θ Cen squared visibilities and UD models. From bottom to top: α Cen A, α Cen B and θ Cen (primary calibrator). The angular diameter of θ Cen was measured using 58 Hya as secondary calibrator.
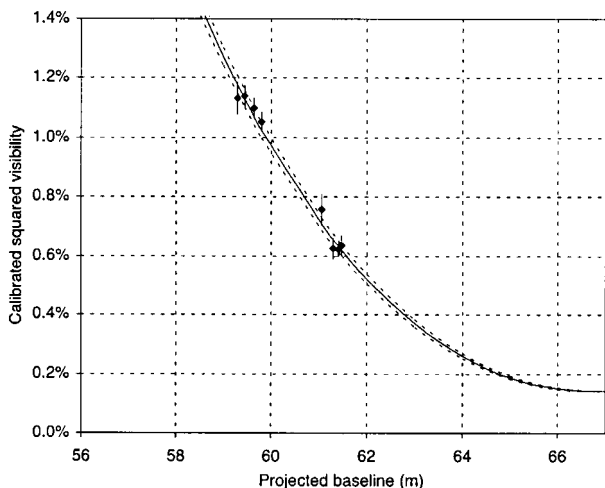
Fig. 7. Detail of α Cen A squared visibility. The continuous line is the uniform disk diameter fit (8.314 ± 0.016 mas), and the dotted lines represent the limits of the $\pm 1\sigma$ error domain. The visibility curve never goes to zero due to the bandwidth smearing effect.
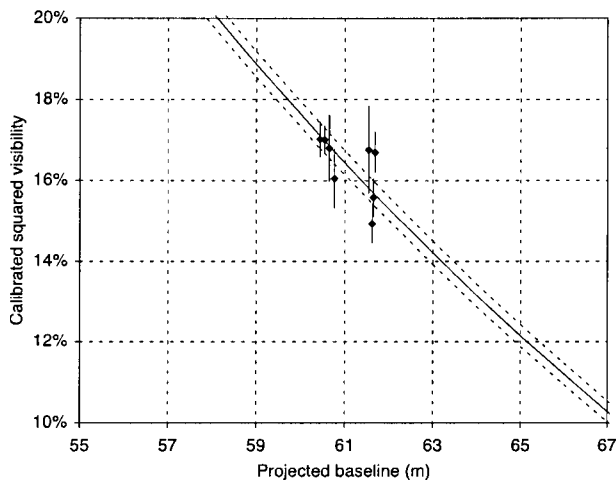
Fig. 8. Detail of α Cen B squared visibility. The continuous line is the uniform disk diameter fit (5.856 ± 0.027 mas), and the dotted lines represent the limits of the $\pm 1\sigma$ error domain.

Table 5. α Cen A squared visibilities, expressed in percents.

JD − 2 450 000	B (m)	Azim. ($N = 0$)	V^2 (%) ± stat. ± syst.
E0-G0			
1988.78108	15.9201	64.95	78.99 ± 1.48 ± 2.81
1988.78380	15.9071	65.79	79.61 ± 1.46 ± 2.83
1988.78652	15.8930	66.62	79.82 ± 1.42 ± 2.84
1988.78901	15.8793	67.39	79.80 ± 1.47 ± 2.84
1995.76493	15.9058	65.86	80.15 ± 1.03 ± 0.66
1996.63335	15.7916	24.31	78.66 ± 1.10 ± 0.42
1996.63970	15.8129	26.48	82.19 ± 1.12 ± 0.44
1996.64733	15.8390	29.06	80.33 ± 1.29 ± 0.43
1996.65492	15.8650	31.61	81.49 ± 1.15 ± 0.44
1996.67842	15.9399	39.40	80.87 ± 1.10 ± 0.43
1996.68327	15.9532	40.99	79.40 ± 1.10 ± 0.43
2001.80688	15.3644	83.76	80.71 ± 1.94 ± 0.05
2001.80954	15.3273	84.59	82.77 ± 2.69 ± 0.04
2002.70376	16.0062	52.80	78.76 ± 0.74 ± 0.05
2002.70640	16.0057	53.63	80.01 ± 1.07 ± 0.05
2003.83537	14.8150	94.44	82.49 ± 1.10 ± 0.05
2003.83780	14.7695	95.22	82.01 ± 1.80 ± 0.04
2003.84099	14.7088	96.25	85.30 ± 1.28 ± 0.05
2003.84356	14.6589	97.08	83.64 ± 1.77 ± 0.04
E0-G1			
2462.55258	59.2848	150.05	1.132 ± 0.051 ± 0.017
2462.55613	59.4391	150.91	1.139 ± 0.032 ± 0.017
2462.56087	59.6365	152.05	1.099 ± 0.031 ± 0.017
2462.56493	59.7975	153.04	1.054 ± 0.029 ± 0.016
2465.61044	61.2943	166.21	0.626 ± 0.035 ± 0.010
2470.58454	61.0497	163.19	0.758 ± 0.052 ± 0.012
2470.60337	61.4043	167.84	0.624 ± 0.023 ± 0.010
2470.60778	61.4696	168.93	0.637 ± 0.033 ± 0.010

Table 6. α Cen B squared visibilities.

JD − 2 450 000	B (m)	Azim. ($N = 0$)	V^2 (%) ± stat. ± syst.
E0-G1			
2462.58356	60.4413	157.57	17.02 ± 0.36 ± 0.26
2462.58697	60.5443	158.40	17.01 ± 0.23 ± 0.26
2462.59047	60.6453	159.26	16.80 ± 0.77 ± 0.26
2462.59490	60.7665	160.35	16.05 ± 0.68 ± 0.24
2465.62682	61.5409	170.27	16.76 ± 1.05 ± 0.26
2470.62033	61.6208	172.05	14.94 ± 0.44 ± 0.23
2470.62342	61.6500	172.82	15.59 ± 0.42 ± 0.24
2470.62783	61.6866	173.92	16.70 ± 0.44 ± 0.25

Table 7. Uniform disk angular diameters of α Cen A and B in the K band derived from the VINCI/VLTI observations.

	α Cen A	α Cen B
θ_{UD} (mas)	8.314 ± 0.016	5.856 ± 0.027

purpose, the PSD of the stellar fringes is computed numerically over the K band using 10 nm spectral bins. We take here into account the total transmission of the interferometer

and the visibility of the fringes for each wavelength. The total power is then integrated and gives a numerical broadband visibility function $V_K{}^2(B, \theta_{UD})$ where B is the projected baseline, and θ_{UD} the UD angular diameter. To derive the α Cen UD diameters, we make a classical χ^2 minimization between our $(B, V_K{}^2)$ measurements and the $V_K{}^2(B, \theta_{UD})$ function while changing the value of θ_{UD}.

Figure 6 shows the complete visibility curve of the UD model fit to the α Cen data, together with the primary calibrator θ Cen. The detail of the visibility curve of α Cen A shown in Fig. 7 demonstrates that the visibility never goes down to zero for any baseline, due to the bandwidth smearing effect. The minimum squared visibility is 0.15%, for a baseline length of aproximately 66.5 m. Figure 8 shows an enlargement of the visibility points obtained on α Cen B. The final UD angular diameters for the two stars and the corresponding effective wavelengths are given in Table 7.

7.2. Limb darkened angular diameters

In this section, we describe two methods to compute the LD angular diameter: through a conversion factor (classical approach), and through a visibility fit taking directly the limb darkening into account.

7.2.1. LD/UD conversion factor

The simplest approach to retrieve the limb darkened diameter from an interferometric UD measurement goes through the computation of the conversion factor ρ defined by:

$$\rho = \frac{\theta_{LD}}{\theta_{UD}} \tag{3}$$

ρ is deduced from stellar atmosphere luminosity profiles that are computed using radiative transfer modeling codes. These profiles are published in tables as a function of the wavelength band (e.g. Claret 2000). One limitation of the description of the LD visibility curve of the star by a single parameter is that it assumes that the visibility curve of the UD and LD models have the same intrinsic shape. This is not exactly the case near and especially after the first minimum of the visibility function. However, this approximation is satisfactory for compact stellar atmospheres such as the ones of α Cen stars. Hanbury Brown et al. (1974) have shown that the linear limb darkening coefficient u can be translated into the conversion factor ρ through the approximate formula:

$$\rho = \sqrt{\frac{1 - u/3}{1 - 7u/15}}. \tag{4}$$

These authors quote a maximum error of ±0.2% for this approximate formula, that is in general very satisfactory, but for the particular case of α Cen A, this uncertainty is comparable to our final error bar on the UD diameter. Different values of linear limb darkening conversion factors are given in Table 8, based on successive versions of the Claret et al. models (1995, 1998, 2000). Except for the older Claret (1995) values, that do

Table 8. Linear LD/UD conversion factors for α Centauri. The assumed physical parameters to match Claret's (2000) grid are the closest ones to those of Thévenin et al. (2002).

Model from Claret (2000)	α Cen A	α Cen B
$T_{\rm eff}$ (K)	5750	5250
$\log(g)$ (cm s^{-2})	4.5	4.5
$\log(M/H)$ (dex)	0.2	0.2
V_T (km s^{-1})	2.0	2.0
Reference	ρ_A	ρ_B
Claret et al. (1995)	102.047%	102.299%
Claret (1998)	102.388%	102.723%
Claret (2000)	102.355%	102.635%

not take metallicity and turbulence velocity into account, the two other results are very close to each other.

In order to account for a possible systematic error in the determination of the limb darkening parameter, we allow a ±0.1% uncertainty to propagate into the computation of the limb darkened diameter of α Cen. It should be noted that the coefficients for both stars originate from the same Kurucz's model atmosphere computations of Claret (2000), and are therefore likely to have a good intrinsic consistency.

7.2.2. Limb darkened disk visibility fit

Hestroffer (1997) has chosen another approach by computing the analytical expression of the visibility function for a single-parameter power law intensity profile $I_\lambda(\mu) = \mu^\alpha$ (with $\alpha \geq 0$) where $\mu = \cos(\theta)$ is the cosine of the azimuth of a surface element of the star. This simplification allows this author to derive the analytical expression of the visibility function corresponding to a power law limb darkened disk:

$$V_\nu(x) = \Gamma(\nu + 1) \frac{J_\nu(x)}{(x/2)^\nu} \tag{5}$$

where $x = \pi B \theta / \lambda$ is the spatial frequency, $\nu = \alpha/2 + 1$, and $J_\nu(x)$ is the Bessel function of the first kind. As the intensity profiles produced by the most recent atmosphere models are close to power laws, as shown in Fig. 9, the power law fitting procedure gives good results. Claret (2000) has computed a four parameters law that aproximates very well the most recent Kurucz models for observations in the K band. Using this law gives a value of $\alpha = 0.1417$ for α Cen A and $\alpha = 0.1598$ for α Cen B.

The final precision on ρ is better than with the previous linear approximation, but as for the conversion coefficient approach presented in Sect. 7.2.1, we propagate an uncertainty of ±0.1% to the final LD angular diameter to account for a possible bias.

Practically, the fit is achieved on the calibrated visibilities listed in Tables 5 and 6 by a classical χ^2 minimization procedure. The product of this fit is directly the LD angular diameter of the star, without the intermediate step of the uniform disk model.
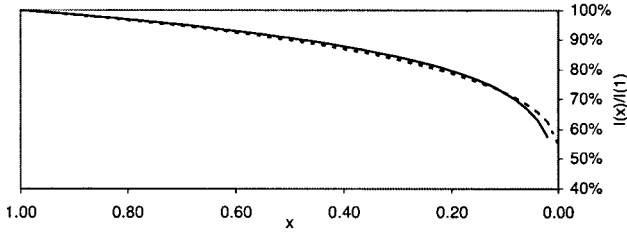
Fig. 9. Intensity profile of α Cen A from the four-parameters limb darkening law of Claret (2000) (dashed line) and the corresponding $\alpha = 0.1417$ power law.

Table 9. Summary of limb-darkened angular diameters from different computation methods. Both methods are based on the Claret (2000) coefficients. The fitting results using the analytical Hestroffer (1997) formula are assumed in the rest of this paper.

LD computation method	α Cen A (mas)
Hanbury Brown et al. (1974)	8.517 ± 0.021
Hestroffer (1997) analytical	**8.511 ± 0.020**
	α Cen B (mas)
Hanbury Brown et al. (1974)	6.010 ± 0.030
Hestroffer (1997) analytical	**6.001 ± 0.034**

7.3. Rotational distortions

As the VINCI/VLTI measurements have been obtained mostly at the same azimuth (roughly N-S), a possible source of bias could be the presence of flattening on the stellar disks due to rotational distortion. The estimated equatorial rotation periods for α Cen A and B are 22 and 41 days respectively (Morel et al. 2000), bracketing the solar value. The corresponding small rotational velocities rule out any flattening at a significant level, and therefore no correction has been applied to our measurements.

7.4. Summary of angular diameter values

Table 9 gives the limb darkened angular diameters derived from the LD/UD conversion factors and from the analytical LD visibility function (Hestroffer 1997). This last method is assumed in the following sections. All values take the bandwidth smearing effect into account.

8. Comparison of asteroseismic and interferometric linear diameters

8.1. Parallax from the literature

To convert the angular diameter into a linear value, it is necessary to know the parallax of the star. The α Cen system being very nearby ($D = 1.3$ pc), the precision on the measurement of its trigonometric parallax is potentially very good. Unfortunately, some discrepancies have appeared between the most recently published values (Table 10). In particular, the original *Hipparcos* parallax (Perryman et al. 1997) and the value by Pourbaix et al. (1999) are significantly different from the reprocessing of the *Hipparcos* data by Söderhjelm (1999), by more than 3σ. A difficulty with the *Hipparcos* satellite

Table 10. Parallax values of α Cen from the litterature.

Value (mas)	Author
750	Heintz (1958, 1982)
749 ± 5	Kamper & Wesselink (1978)
750.6 ± 4.6	Demarque et al. (1986)
742.1 ± 1.4	Perryman et al. (1997)
737.0 ± 2.6	Pourbaix et al. (1999)
747.1 ± 1.2	Söderhjelm (1999)

measurement is due to the large brightness of the α Cen pair. The light from one of the stars possibly contaminated the measurement on the other, leading to a systematic bias that may not have been propagated properly to the final error bars. In Sect. 8.2, we adopt the parallax value from Söderhjelm (1999), who took this effect into account.

As a remark, the semi-major axis of the orbit of the two stars $a = 17.59 \pm 0.03$ AU (Pourbaix et al. 1999) is totally negligible compared to the distance D to the couple ($a/D = 0.006\%$), therefore the two stars can be considered at the same distance.

8.2. Linear diameters

Considering the parallax of 747.1 ± 1.2 mas from Söderhjelm (1999), it is now possible to compute the linear diameters of α Cen A and B (in solar units) from the two LD angular diameters determined interferometrically. They are found to be:

$$D[A] = 1.224 \pm 0.003 \, D_{\odot} \tag{6}$$

$$D[B] = 0.863 \pm 0.005 \, D_{\odot} \tag{7}$$

and can be compared to the linear diameters proposed by Thévenin et al. (2002):

$$D[A] = 1.230 \pm 0.003 \, D_{\odot} \tag{8}$$

$$D[B] = 0.857 \pm 0.007 \, D_{\odot} \tag{9}$$

The theoretical diameters are only $+1.3\sigma$ and -0.7σ away from the observed values. Both interferometric diameters and those deduced from the photometric calibration constrained by asteroseismic frequencies therefore agree very well.

These two model diameters are derived using the CESAM code, and are defined as the radii at which the temperature in the atmosphere is equal to the effective temperature of the star. Computing the layer where the continuum at $2.2 \, \mu$m is formed leads to temperatures close to $T_{\rm eff}$, therefore the CESAM diameters can be directly compared to those measured by the VLTI at $2.2 \, \mu$m.

8.3. Self consistent parallax

From our angular diameter measurements and the asteroseismic diameter estimations, we can also derive directly the parallax of the couple. The simple formula linking the limb darkened angular diameter $\theta_{\rm LD}$ (in mas), the linear diameter D (in $D_{\odot}$) and the parallax π (in mas) is:

$$\theta_{\rm LD} = 9.305 \times 10^{-3} \, D \, \pi. \tag{10}$$

Table 11. Parallax of α Cen from VINCI/VLTI and asteroseismological observations, and the corresponding self-consistent stellar parameters. Linear diameters are taken from the asteroseismology study by Thévenin et al. (2002).

Derived parallax	745.3 ± 2.5 mas	
	α Cen A	α Cen B
VINCI LD size (mas)	8.511 ± 0.020	6.001 ± 0.034
Model LD size (mas)	8.530 ± 0.035	5.943 ± 0.052
VINCI diameter ($D_\odot$)	1.227 ± 0.005	0.865 ± 0.006
Model diameter ($D_\odot$)	1.230 ± 0.003	0.857 ± 0.007

A least squares fit is computed between the LD angular diameters from the VLTI and the linear diameters from Thévenin et al. (2002). We find an optimal parallax of 745.3 ± 2.5 mas, that differs slightly from the original *Hipparcos* value by +1.1σ (Perryman et al. 1997), from Pourbaix et al. (1999) by +2.3σ, and from Söderhjelm (1999) by only −0.7σ. The resulting values of angular and linear diameters are given in Table 11. The difference between theoretical and linear diameters for the self-consistent parallax is limited to +0.5σ and −0.9σ, respectively for α Cen A and B.

8.4. Ratio of α Cen A and B radii

Contrary to the linear diameters themselves, their ratio is independent of the actual parallax of the system. Therefore, part of the systematic uncertainties can be removed by using this observable as a comparison basis between the observations and the models. For α Cen A and B, we have access to a very good quality parallax, and the uncertainty introduced there is relatively small. On the other hand, when measuring a farther double or multiple star, the parallax may be unknown, or known only with a bad precision. In this case, comparing the ratio of the stellar diameters will give much stronger constraints to the stellar structure models than the individual values. This technique is also applicable to the interferometric measurement of stars in clusters, within which the distance can be assumed to be uniform. From the limb-darkened values listed in Table 9, we obtain the following ratio between the angular diameters of α Cen A and B:

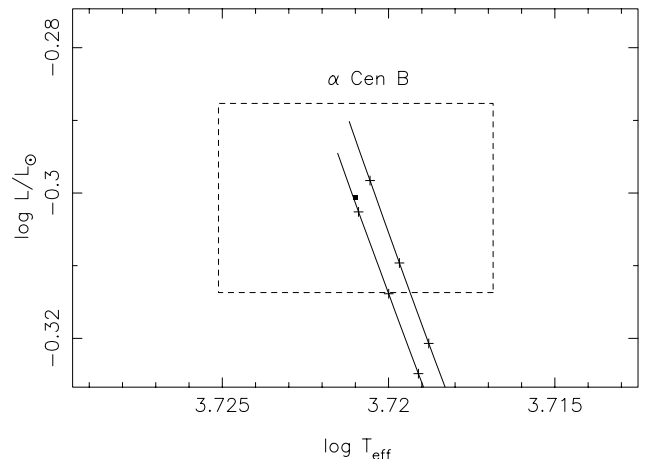$$\frac{\theta_{\mathrm{LD}}[A]}{\theta_{\mathrm{LD}}[B]} = 1.418 \pm 0.009. \tag{11}$$

This value can be compared to the ratio of linear radii from the Thévenin et al. (2002) models that is:

$$\frac{R[A]}{R[B]} = 1.435 \pm 0.014. \tag{12}$$

We therefore find a slight diameter excess of α Cen B at a level of 1.0σ.

8.5. Masses and evolutionary models

As emphasized by Thévenin et al. (2002), the seismological analysis gives strong constraints on masses and on the age of

Fig. 10. HR diagram of α Cen B. The line on the right corresponds to a mixing length of $\lambda = 0.96$ and a mass of 0.909 $M_\odot$, the line on the left corresponds to the values published in Thévenin et al. 2002 ($\lambda = 0.98$, 0.907 $M_\odot$).

the system when combined with spectro-photometric measurements. To achieve this, one derives from the set of oscillation frequencies, one "large" and two "small" frequency spacings. The large frequency spacing is a difference between frequencies of modes with consecutive radial order n: $\Delta\nu_\ell(n) \equiv \nu_{n,\ell} - \nu_{n-1,\ell}$. In the high frequency range, i.e. large radial orders, $\Delta\nu_\ell$ is almost constant with a mean value $\Delta\nu_0$, strongly related to the mean density of the star, i.e. to the mass and the radius. The small separations are very sensitive to the physical conditions in the core of the star and consequently to its age. These frequencies measured for the star A have largely forced the spectro-photometric calibration to decrease the masses of the stellar system α Cen, leading to the following values: $M_A = 1.100 \pm 0.006 \, M_\odot$ and $M_B = 0.907 \pm 0.006 \, M_\odot$ (Thévenin et al. 2002) close to those adopted by Guenther & Demarque (2000) and Kim (2000). The mass of the B component departs significantly by 3% from the value published by Pourbaix et al. (2002).

Using the orbital properties of the binary and also spectro-velocimetric curves, Pourbaix et al. (2002) have derived the masses of each components ($M_A = 1.105 \pm 0.007 \, M_\odot$, $M_B = 0.934 \pm 0.006 \, M_\odot$). We note that Thoul et al. (2003) have recently proposed a model of the binary system using these masses and spectro-photometric constraints different from that of Thévenin et al. (2002). They were able to reproduce the seismic frequencies of α Cen A, but the model they propose does not take into account the helium and heavy elements diffusion.

Because the interferometric diameter of α Cen B is a little larger than those deduced from the CESAM model, we explored the possibility to decrease this difference by changing the mixing length of the B model from $\lambda = 0.98$ to $\lambda = 0.96$, and by increasing the mass of the star from 0.907 to 0.909 $M_\odot$. These modifications do not change the calibration of α Cen A. We took care in this process to keep the star B in its error box on the HR diagram (Fig. 10). It results from this new mass a diameter that is closer to the interferometric one: 0.863 $D_\odot$ or 5.999 ± 0.050 mas (parallax from Söderhjelm 1999). The effective temperature is found to be 5262 K, identical to the

adopted spectroscopic one T_{eff} = 5260 K. Our results confirm that the mass of the B component is probably close to 0.907 $M_{\odot}$, as reported by Thévenin et al. (2002). A similar exercice is not possible if we adopt the mass of 0.934 $M_{\odot}$ derived by Pourbaix et al. (2002).

9. Conclusion

We have determined the angular diameters of α Cen A and B using the VINCI/VLTI instrument, to a relative precision of 0.2% and 0.6%, respectively. The low values of the α Cen A visibilities allowed us to match our statistical visibility error to the calibration uncertainty. This is an optimal situation for the angular diameter measurement, that would not have been feasible with a higher visibility. Calibrating with a fainter and smaller unresolved star would also not have been efficient, as we would have degraded significantly our statistical precision. There is still a compromise, as the low visibilities of α Cen A imply a slightly degraded statistical precision, but E0-G1 has proved to be a well suited baseline for the simultaneous measurement of the angular diameters of α Cen A and B.

The comparison of these interferometric diameters with the values derived using asteroseismic constraints shows a good agreement when adopting the parallax determined by Söderhjelm (1999). In particular, our diameters are compatible with the masses proposed by Thévenin et al. (2002) for both stars. In the near future, asteroseismic observations of the large frequencies spacing $\Delta\nu_{\ell}$ of α Cen B will complete the calibration of this binary system. Simultaneously, the very long baselines of the VLTI (up to 200 m) will allow us to measure directly the limb darkening of these two stars, and therefore derive the photospheric diameter without using a stellar atmosphere model. This work demonstrates that the combination of the interferometry and asteroseismology techniques can provide strong constraints on stellar masses and other fundamental parameters of stars.

References

Berger, J.-P., Haguenauer, P., Kern, P., et al. 2001, A&A, 376, 31

Bordé, P., Coudé du Foresto, V., Chagnon, G., & Perrin, G. 2002, A&A, 393, 183

Bouchy, F., & Carrier, F. 2001, A&A, 374, L5

Bouchy, F., & Carrier, F. 2002, A&A, 390, 205

Bouchy, F., & Carrier, F. 2002, Eddington Workshop, ESA SP-485, 253

Cayrel de Strobel, G., Soubiran, C., Friel, E. D., Ralite, N., & Francois, P. 1997, A&AS, 124, 299

Claret, A., Diaz-Cordovez, J., & Gimenez, A. 1995, A&AS, 114, 247

Claret, A. 1998, A&A, 335, 647

Claret, A. 2000, A&A, 363, 1081

Cohen, M., Walker, R. G., Carter, B., et al. 1999, AJ, 117, 1864

Coudé du Foresto, V., Ridgway, S., & Mariotti, J.-M. 1997, A&AS, 121, 379

Demarque, P., Guenter, D. B., & van Altena, W. F. 1986, ApJ, 300, 773

Evans, J. W., & Michard, R. 1962, ApJ, 136, 493

Farge, M. 1992, Ann. Rev. Fluid Mech., 24, 395

Glebocki, R., Gnacinski, P., & Stawikowski, A. 2000, Acta Astron., 50, 509

Glindemann, A., Abuter, R., Carbognani, F., et al. 2000, SPIE, 4006, 2

Guenther, D. B., & Demarque, P. 2000, ApJ, 531, 503

Hanbury Brown, R., Davis, J., Lake, R. J. W., & Thompson, R. J. 1974, MNRAS, 167, 475

Heintz, W. 1958, Veröff. Münch. Observ., 5, 100

Heintz, W. 1982, Veröff. Münch. Observ., 102, 42

Hestroffer, D. 1997, A&A, 327, 199

Kamper, K. W., & Wesselink, A. J. 1978, AJ, 83, 1653

Kervella, P., Coudé du Foresto, V., Glindemann, A., & Hofmann, R. 2000, SPIE, 4006, 31

Kervella, P., Gitton, Ph., Ségransan, D., et al. 2003a, SPIE, 4838, 858

Kervella P., Ségransan, D., & Coudé du Foresto, V. 2003b, in preparation

Kim, J. C. 1999, JKAS, 32, 119

Leighton, R. B. 1960, in Proc. IAU Symp., 12, 321

Leinert, C., Graser, U., Waters, L. B. F. M., et al. 2000, SPIE, 4006, 43

Lord, S. D. 1992, NASA Technical Memor. 103957, data available at http://www.gemini.edu

Morel, P. 1997, A&AS, 124, 597

Morel, P., Provost, J., Lebreton, Y., Thévenin, F., & Berthomieu, G. 2000, A&A, 363, 675

Morel, P., Berthomieu, G., Provost, J., & Thévenin, F. 2001, A&A, 379, 245

Perrin G., 2003, A&A, 398, 385

Perryman, M. A. C., Lindegren, L., Kovalevsky, J., et al. 1997, A&A, 323, 49

Petrov, R., Malbet, F., Richichi, A., et al. 2000, SPIE, 4006, 68

Pourbaix, D., Neuforge-Verheecke, C., & Noels, A. 1999, A&A, 344, 172

Pourbaix, D., Nidever, D., McCarthy, C., et al. 2002, A&A, 386, 280

Ségransan, D., Forveille, T., Millan-Gabet, C. P. R., & Traub, W. A. 1999, in ASP Conf. Ser., 194, 290

Ségransan, D., Kervella, P., Forveille, T., & Queloz, D. 2003, A&A, 397, L5

Söderhjelm, S. 1999, A&A, 341, 121

Thévenin, F., Provost, J., Morel, P., et al. 2002, A&A, 392, L9

Thoul, A., Scufflaire, R., Noels, B., et al. 2003, A&A, submitted [astro-ph/0303467]